EPJ Web of Conferences **75**, 04010 (2014)
DOI: 10.1051/epjconf/ 201475 04010

Formation of $Sm(Co_{1-x}Ni_x)_5$ epitaxial thin films on Cu(111) underlayers

Makoto Yamada[1,a], Takato Yanagawa[1], Yusuke Hotta[1], Mitsuru Ohtake[1], Fumiyoshi Kirino[2], and Masaaki Futamoto[1]

[1]Faculty of Science and Engineering, Chuo University, 1-13-27 Kasuga, Bunkyo-ku, Tokyo 112-8551, Japan
[2]Graduate School of Fine Arts, Tokyo University of the Arts, 12-8 Ueno-koen, Taito-ku, Tokyo 110-8714, Japan

Abstract. $Sm_{17}(Co_{1-x}Ni_x)_{83}$ (at. %, x = 0, 0.2, 0.8, 1) alloy thin films are prepared on Cu(111) underlayers hetero-epitaxially grown on MgO(111) substrates by molecular beam epitaxy. The effects of substrate temperature and Ni/Co composition on the growth behavior and the detailed resulting film structure are investigated. Formation of RT_5 ordered phase is enhanced with increasing the substrate temperature and the Ni composition. The long-range order degrees of $Sm_{17}Co_{83}$, $Sm_{17}(Co_{0.8}Ni_{0.2})_{83}$, $Sm_{17}(Co_{0.2}Ni_{0.8})_{83}$, and $Sm_{17}Ni_{83}$ films deposited at 500 °C are estimated to be 0.77, 0.82, 0.89, and 0.97, respectively. The $Sm_{17}(Co_{1-x}Ni_x)_{83}$ films with RT_5 structure consist of two types of epitaxial (0001) variant whose orientations are rotated around the film normal by 30° each other. With increasing the Ni content ratio of x from 0 to 1, the volume ratio of two variants is varied from 53:47 to 94:6. The nucleation of only one-type variant with a smaller lattice mismatch with respect to Cu underlayer is promoted with increasing the Ni content ratio.

1 Introduction

$SmCo_5$ alloy with RT_5 ($D2_d$) ordered structure shows K_u of 1.1×10^8 erg/cm^3 [1] and the thin films with the c-axis perpendicular to the substrate surface have been investigated for applications like future recording media with the areal density exceeding 1 Tb/in^2. $SmCo_5$ polycrystalline [2–7] and epitaxial [8–10] films of (0001) orientation have been prepared on Cu [2–5,8,9], Cu/Ti [4,5], Ru/Cu/Ru [6], Ru [7,10], and Ru-Cr [7] underlayers. Most of the samples include a Cu underlayer. It is reported that Cu atoms of underlayer diffuse into an Sm-Co film and partially substitute the Co site in $SmCo_5$ structure forming an alloy compound of $Sm(Co,Cu)_5$ [4,5]. The dissolution of Cu atom into Sm-Co alloy is known to stabilize RT_5 structure [11–13].

The Co site in $SmCo_5$ structure can be replaced with a 3d ferromagnetic transition metal element of T = Ni [14]. The crystallization temperature and the film structure are considered to vary depending on the T element. Ni (1455 °C) has a lower melting point than Co (1495 °C). Ni atoms are thus considered to diffuse more easily and to have a lower activation energy in forming the SmT_5 compound. In our previous studies [8,9], $SmCo_5$ epitaxial films were prepared on Cu(111) underlayers by employing a molecular beam epitaxy (MBE) system equipped with a reflection high-energy electron diffraction (RHEED) facility. *In-situ* observations revealed the crystallographic property during film formation. In the present study, $Sm_{17}(Co,Ni)_{83}$ and $Sm_{17}Ni_{83}$ (at. %) films are deposited on Cu(111) underlayers in addition to $Sm_{17}Co_{83}$ films. The effects of Ni/Co composition and substrate temperature on the ordered phase formation are investigated.

2 Experimental procedure

Thin films were prepared on MgO(111) substrates at temperatures ranging from 100 to 500 °C by using an MBE system with the base pressures lower than 7×10^{-9} Pa. Substrates were heated at 500 °C for 1 h before film formation to obtain clean surfaces. Co, $Co_{80}Ni_{20}$, $Co_{20}Ni_{80}$ alloy, and Ni materials were evaporated by electron beam heating, whereas Sm and Cu were evaporated by using Knudsen cells. The purities of evaporation sources were higher than 99.9%. The film layer structure is $Sm_{17}(Co_{1-x}Ni_x)_{83}$(20 nm)/Cu(20 nm)/MgO. A 20-nm-thick Cu underlayer and a 20-nm-thick $Sm_{17}(Co_{1-x}Ni_x)_{83}$ (x = 0, 0.2, 0.8, 1) films were sequentially deposited on the substrate. The epitaxial orientation relationship of Cu underlayer with respect to substrate [8,9] was Cu(111)[1 $\bar{1}$ 0], [$\bar{1}$ 10] ∥ MgO(111)[1 $\bar{1}$ 0]. The Cu underlayer consisted of two epitaxial fcc(111) variants whose atomic stacking sequences of close-packed plane along the perpendicular direction were ABCABC… and ACBACB… The $Sm_{17}(Co_{1-x}Ni_x)_{83}$ film was deposited by co-evaporation of Sm and $Co_{100(1-x)}Ni_{100x}$ materials. The compositions of $Sm_{17}(Co_{1-x}Ni_x)_{83}$ films were confirmed by energy dispersive X-ray spectroscopy and the errors were less than 2 at. % from the $Sm(Co_{1-x}Ni_x)_5$ stoichiometries.

The surface structure during film deposition was studied by RHEED. The resulting film structure was investigated by $2\theta/\omega$-scan out-of-plane, $2\theta\chi/\varphi$-scan in-plane, and β-scan pole-figure X-ray diffractions (XRDs) with Cu-Kα radiation (λ = 0.15418 nm).

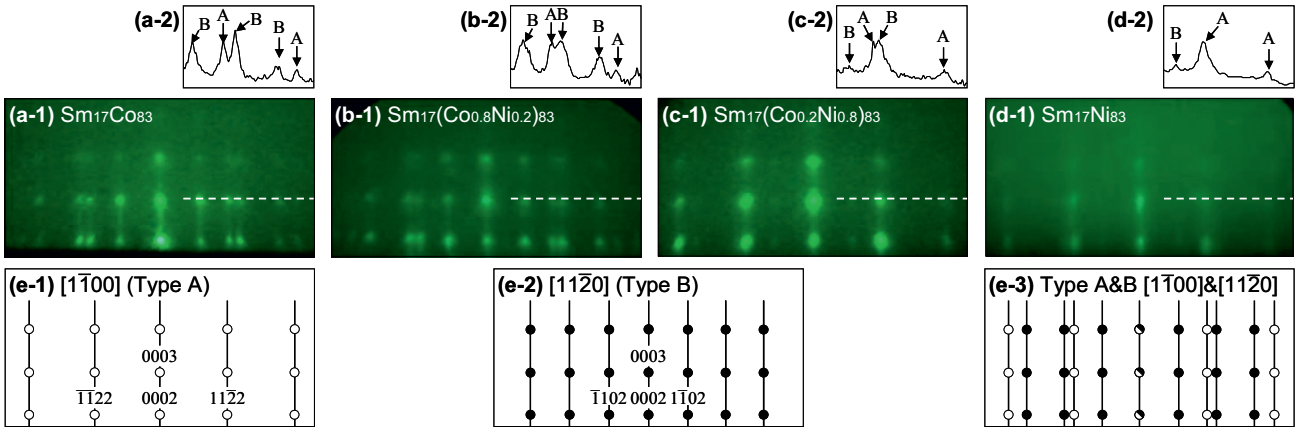

Fig. 1. (a-1)–(d-1) RHEED patterns and (a-2)–(d-2) the schematic diagrams of (a) $Sm_{17}Co_{83}$, (b) $Sm_{17}(Co_{0.8}Ni_{0.2})_{83}$, (c) $Sm_{17}(Co_{0.2}Ni_{0.8})_{83}$, and (d) $Sm_{17}Ni_{83}$ films of 20 nm thickness deposited on Cu(111) underlayers at 500 °C. The profiles of (a-2)–(d-2) are measured along the dotted lines in (a-1)–(d-1). (e) Schematic diagrams of RHEED patterns simulated for (0001) surfaces with RT_5 ordered structure. The incident electron beam is parallel to (a)–(d) MgO[11$\bar{2}$], (e-1) [1$\bar{1}$00], or (e-2) [11$\bar{2}$0].

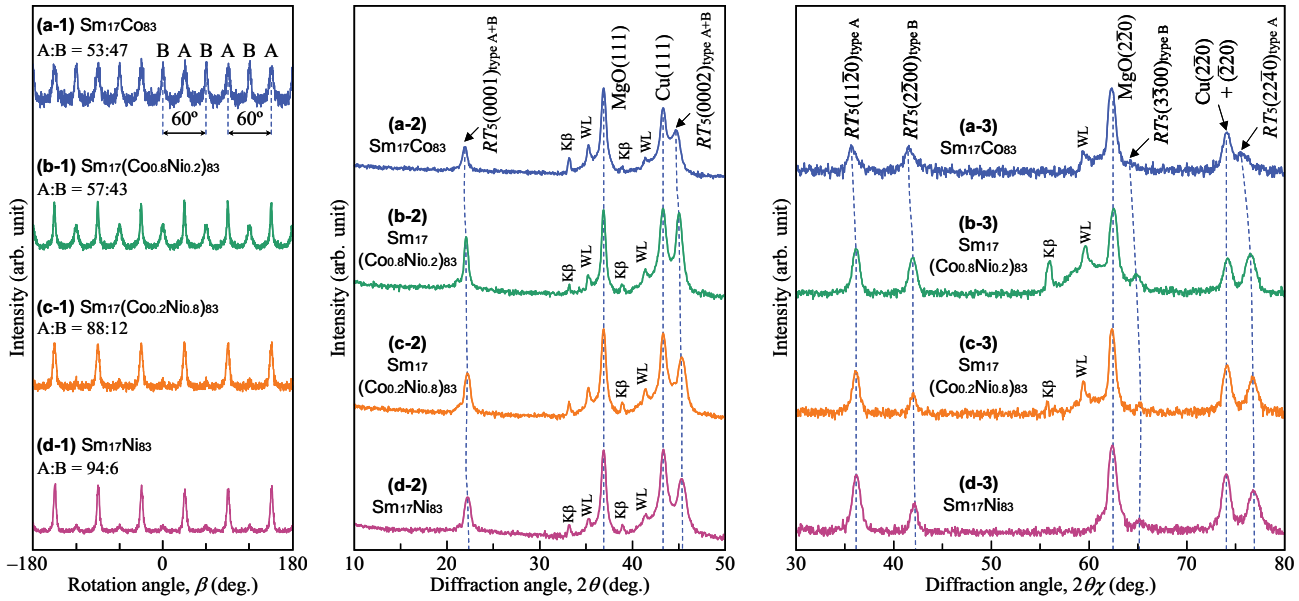

Fig. 2. (a-1)–(d-1) Pole-figure, (a-2)–(d-2) out-of-plane, and (a-3)–(d-3) in-plane XRD patterns of (a-1)–(a-3) $Sm_{17}Co_{83}$, (b-1)–(b-3) $Sm_{17}(Co_{0.8}Ni_{0.2})_{83}$, (c-1)–(c-3) $Sm_{17}(Co_{0.2}Ni_{0.8})_{83}$, and (d-1)–(d-3) $Sm_{17}Ni_{83}$ films deposited on Cu(111) underlayers at 500 °C. The pole-figure patterns are measured by fixing the tilt and diffraction angles of (α, $2\theta B$) at (47°, 30.5°). The in-plane patterns are measured by making the scattering vector parallel to MgO[1$\bar{1}$0]. The intensity is shown in (a-1)–(d-1) a linear scale or (a-2)–(d-3) a logarithmic scale. The small reflections noted as Kβ and WL are due to Cu-Kβ and W-Lα radiations included in the X-ray source, respectively.

3 Results and discussion

The effects of Co/Ni composition on the growth behaviour and the film structure were investigated. Here, the substrate temperature was fixed at 500 °C. Figures 1(a-1)–(d-1) show the RHEED patterns of $Sm_{17}(Co_{1-x}Ni_x)_{83}$ films deposited on Cu(111) underlayers observed by making the incident electron beam parallel to MgO[11$\bar{2}$] (|| Cu[11$\bar{2}$], [$\bar{1}$1$\bar{2}$]). Clear diffraction patterns corresponding to RT_5(0001) texture [figure 1(e-3)] are observed for all the films. Epitaxial $Sm_{17}(Co_{1-x}Ni_x)_{83}$ films with RT_5 ordered structure and with the c-axis perpendicular to the substrate surface are obtained. The diffraction patterns are analyzed to be an overlap of two reflections [figures 1(e-1, e-2)], as shown by the arrows A and B in the intensity profiles of figures (a-2)–(d-2). The epitaxial orientation relationship is thus determined as follows,

$Sm_{17}(Co_{1-x}Ni_x)_{83}(0001)[1\bar{1}00]$
|| Cu(111)[11$\bar{2}$], [$\bar{1}$1$\bar{2}$] (type A),
$Sm_{17}(Co_{1-x}Ni_x)_{83}(0001)[11\bar{2}0]$
|| Cu(111)[11$\bar{2}$], [$\bar{1}$1$\bar{2}$] (type B).

The films consist of two types of (0001) variant whose orientations are rotated around the film normal by 30° each other.

In these configuration, the lattice misfit values of A-type $Sm_{17}Co_{83}$, $Sm_{17}(Co_{0.8}Ni_{0.2})_{83}$, $Sm_{17}(Co_{0.2}Ni_{0.8})_{83}$, and $Sm_{17}Ni_{83}$ variants with respect to Cu underlayer are –2.5%, –2.8%, –3.4%, and –3.6%, while those of B-type variants are +12.5%, +12.3%, +11.5%, and +11.3%. Here, the lattice constants of bulk $SmCo_5$ (a_{SmCo5} = 0.4982 nm [15]), $SmNi_5$ (a_{SmNi5} = 0.4926 nm [16]), and Cu (a_{Cu} = 0.3615 nm [17]) crystals and the lattice constants of $a_{SmCo4Ni}$ (= $0.8a_{SmCo5}$+$0.2a_{SmNi5}$) and $a_{SmCoNi4}$ (= $0.2a_{SmCo5}$+$0.8a_{SmNi5}$), which are estimated by using the

lattice constants of a_{SmCo5} and a_{SmNi5}, are used. Although there are fairly large mismatches in the cases of B-type variants, epitaxial growth is taking place. With increasing the Ni composition, the intensity of RHEED reflection from B-type variant becomes weaker, as shown in figures 1(a-2)–(d-2). In order to investigate the volume ratio of two types of variant, pole-figure XRD was carried out. Figures 2 (a-1)–(d-1) show the β-scan pole-figure XRD patterns measured by fixing the tilt and diffraction angles of (α, $2\theta B$) at (47°, 30.5°), where $RT_5\{1\bar{1}01\}$ reflections are expected to be detectable. For all the films, twelve $RT_5\{1\,\bar{1}\,01\}$ reflections, which originate from the two types of variant, are observed with 30° separation. The volume ratios of A-type to B-type variant involved in $Sm_{17}Co_{83}$, $Sm_{17}(Co_{0.8}Ni_{0.2})_{83}$, $Sm_{17}(Co_{0.2}Ni_{0.8})_{83}$, and $Sm_{17}Ni_{83}$ films are estimated from the integrated intensities of $\{1\bar{1}01\}$ reflection of each variant to be 53:47, 57:43, 88:12, and 94:6, respectively. The nucleation of only A-type variant is apparently enhanced with increasing the Ni content.

Figures 2(a-2)–(d-2) show the out-of-plane XRD patterns of $Sm_{17}(Co_{1-x}Ni_x)_{83}$ films. $RT_5(0001)$ superlattice reflections are clearly observed in addition to $RT_5(0002)$ fundamental reflections for all the films. The out-of-plane XRD confirms the formation of RT_5 ordered phase. Long-range order degree (S) is estimated by comparing the intensity ratio of $RT_5(0001)$ superlattice to RT_5 fundamental reflection. The intensity (I) is proportional to structure (FF^*), Lorentz-polarization (L), and absorption (A) [18]. Here, I is a product of integrated intensity multiplied by the full with at half maximum of rocking curve measured for the reflection. In the present paper, an influence of temperature factor, which is often omitted when comparing two reflection intensities, is not considered. F_s and F_f are respectively $S[f_{Sm}-\{(1-x)f_{Co}+xf_{Ni}\}]$ and $f_{Sm}+5\{(1-x)f_{Co}+xf_{Ni}\}$ [19], where f is the atomic scattering factor of Sm, Co, or Ni and the subscripts of s and f refer to the superlattice and fundamental reflections, respectively. Therefore, I_s/I_f is expressed as

$$I_{(0001)}/I_{(0002)} = [\{S[f_{Sm}-\{(1-x)f_{Co}+xf_{Ni}\}]\}^2 LA]_s / [f_{Sm}+5\{(1-x)f_{Co}+xf_{Ni}\}^2 LA]_f. \quad (1)$$

By solving this equation, S is given as

$$S = (I_s/I_f)\times\{[f_{Sm}+5\{(1-x)f_{Co}+xf_{Ni}\}]_f / [f_{Sm}-\{(1-x)f_{Co}+xf_{Ni}\}]_s\}\times[\{LA\}_f/\{LA\}_s]^{1/2}. \quad (2)$$

The S values of $Sm_{17}Co_{83}$, $Sm_{17}(Co_{0.8}Ni_{0.2})_{83}$, $Sm_{17}(Co_{0.2}Ni_{0.8})_{83}$, and $Sm_{17}Ni_{83}$ films are 0.77, 0.82, 0.89, and 0.97, respectively. The S value is improved with increasing the Ni content and the $Sm_{17}Ni_{83}$ film is almost fully ordered.

Figures 2(a-3)–(d-3) shows the in-plane XRD patterns measured by making the scattering vector parallel to MgO[1$\bar{1}$0]. $RT_5(11\bar{2}0)$ and $RT_5(22\bar{4}0)$ reflections from A-type variant and $RT_5(2\bar{2}00)$ and $RT_5(3\bar{3}00)$ reflections from B-type variant are recognized. The in-plane XRD confirms the epitaxial orientation relationship determined by RHEED. The lattice constants of A- and B-type variants, ($a_{type\ A}$, $a_{type\ B}$) = ($2d_{(11\bar{2}0)}$, $4/(3^{1/2})d_{(2\bar{2}00)}$), included in $Sm_{17}Co_{83}$, $Sm_{17}(Co_{0.8}Ni_{0.2})_{83}$, $Sm_{17}(Co_{0.2}Ni_{0.8})_{83}$, and $Sm_{17}Ni_{83}$ films are calculated from the in-plane XRD data to be (0.5041 nm, 0.5021 nm), (0.4978 nm, 0.4972 nm), (0.4966 nm, 0.4968 nm), and (0.4964 nm, 0.4959 nm), respectively. The lattice constants, $c_{type\ A+B} = d_{(0001)}$, of $Sm_{17}Co_{83}$, $Sm_{17}(Co_{0.8}Ni_{0.2})_{83}$, $Sm_{17}(Co_{0.2}Ni_{0.8})_{83}$, and $Sm_{17}Ni_{83}$ films are estimated from the out-of-plane XRD data to be 0.4054 nm, 0.4026 nm, 0.4005 nm, and 0.4001 nm, respectively. The lattice constants, $a_{type\ A}$, $a_{type\ B}$, c, of respective films are slightly larger than those of bulk $SmCo_5$ (a_{SmCo5} = 0.4982 nm, c_{SmCo5} = 0.3975 nm [15]), $SmCo_4Ni$ ($a_{SmCo4Ni}$ = 0.4971 nm, $c_{SmCo4Ni}$ = 0.3976 nm), $SmCoNi_4$ ($a_{SmCoNi4}$ = 0.4937 nm, $c_{SmCoNi4}$ = 0.3979 nm), and $SmNi_5$ (a_{SmNi5} = 0.4926 nm, c_{SmNi5} = 0.3980 nm [16]) crystals and smaller than that of bulk $SmCu_5$ (a_{SmCu5} = 0.507 nm, c_{SmCu5} = 0.410 nm [20]) crystal. The T site in $Sm(Co_{1-x}Ni_x)_5$ structure may be partially replaced with Cu atoms with larger atomic radius. There is thus a possibility that Cu atoms of underlayer diffuse into the $Sm_{17}(Co_{1-x}Ni_x)_{83}$ film and an alloy compound of $Sm(Co_{1-x}Ni_x,Cu)_5$ is formed, similar to the case of $SmCo_5$ films formed on Cu underlayers [2–5,8,9].

In order to study the effect of substrate temperature on the ordered phase formation, $Sm_{17}(Co_{1-x}Ni_x)_{83}$ films were deposited at temperatures ranging from 100 to 500 °C. Figures 3(a)–(d) show the RHEED patterns observed during formation of $Sm(Co_{1-x}Ni_x)_5$ films at different temperatures. As the substrate temperature and the Ni

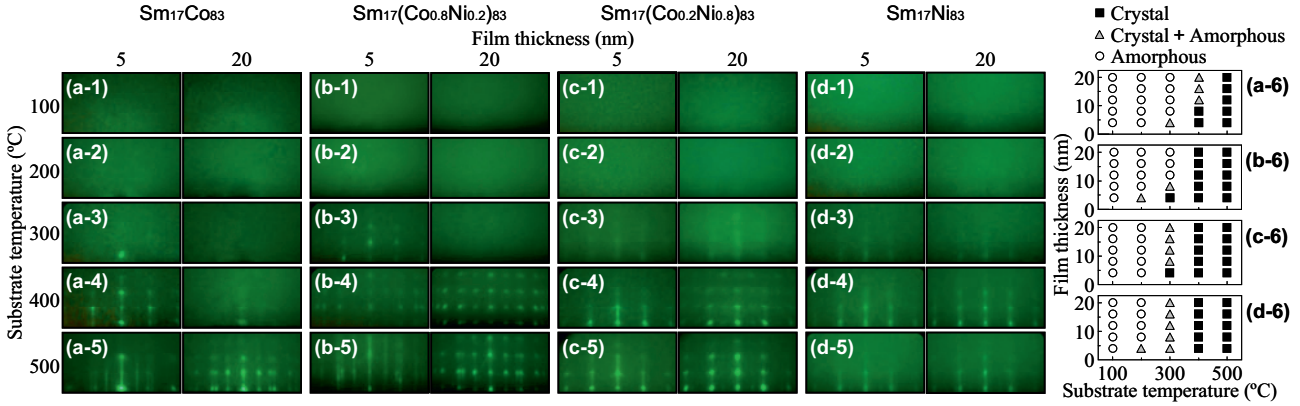

Fig. 3. RHEED patterns observed during formation of (a-1)–(a-5) $Sm_{17}Co_{83}$, (b-1)–(b-5) $Sm_{17}(Co_{0.2}Ni_{0.8})_{83}$, (c-1)–(c-5) $Sm_{17}(Co_{0.8}Ni_{0.2})_{83}$, (d-1)–(d-5) $Sm_{17}Ni_{83}$ films on Cu(111) underlayers at (a-1)–(d-1) 100, (a-2)–(d-2) 200, (a-3)–(d-3) 300, (a-4)–(d-4) 400, and (a-5)–(d-5) 500 °C, respectively. The incident electron beam is parallel to MgO[11$\bar{2}$]. Phase transformation maps of (a-6) $Sm_{17}Co_{83}$, (b-6) $Sm_{17}(Co_{0.2}Ni_{0.8})_{83}$, (c-6) $Sm_{17}(Co_{0.8}Ni_{0.2})_{83}$, and (d-6) $Sm_{17}Ni_{83}$ films.

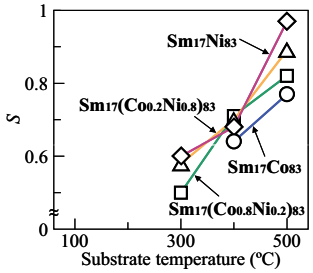

Fig. 4. Substrate temperature dependences on long range ordering parameter, *S* value, measured for $Sm_{17}(Co_{1-x}Ni_x)_{83}$ films.

content decrease from 500 °C and $x = 1$, the sharpness of RHEED pattern gradually decreases with overlapping diffuse contrast. The variation suggests that amorphous phase is appearing. The transformations from crystalline to amorphous phase as functions of film thickness and temperature are summarized in Figs. 3(a-6)–(d-6). The crystallization temperature apparently decreases with increasing the Ni content. The result is possibly due to a lower activation energy of Ni in forming the SmT_5 compound. Figure 4 shows the substrate temperature dependences of *S* of $Sm_{17}(Co_{1-x}Ni_x)_{83}$ films. The *S* value increases with increasing not only the substrate temperature but also the Ni content. A replacement of Co site in $SmCo_5$ structure with Ni atom is useful for enhancing the RT_5 ordered phase formation.

4 Conclusion

$Sm_{17}(Co_{1-x}Ni_x)_{83}$ films are deposited on Cu(111) underlayers by varying the Ni content of x from 0 to 1 and by varying the substrate temperature from 100 to 500 °C. The film growth behavior and the detailed films structure are investigated by RHEED and XRD. With increasing the substrate temperature and the Ni content, formation of RT_5 ordered phase is promoted. The *S* values of $Sm_{17}Co_{83}$, $Sm_{17}(Co_{0.8}Ni_{0.2})_{83}$, $Sm_{17}(Co_{0.2}Ni_{0.8})_{83}$, and $Sm_{17}Ni_{83}$ films are 0.77, 0.82, 0.89, and 0.97, respectively. A replacement of Co site in $SmCo_5$ structure with Ni atom is useful for enhancing the RT_5 ordered phase formation. The $Sm_{17}(Co_{1-x}Ni_x)_{83}$ films consist of two types of (0001) variant. As the Ni content of x increases from 0 to 1, the volume ratio of two variants varies from 53:47 to 94:6. The epitaxial growth of only one-type variant with a smaller lattice mismatch with respect to Cu underlayer is enhanced with increasing the Ni content.

Acknowledgements

A part of this work was supported by JSPS KAKENHI Grant Number 25420294, JST A-STEP Grant Number AS242Z00169M, and Chuo University Grant for Special Research.

References

1. K. J. Strnat, Handbook of Ferromagnetic Materials (Elsevier Science B. V., New York, 1988)
2. J, Sayama, T. Asahi, K. Mizutani, T. Osaka, J. Phys. D **37**, L1 (2004)
3. S. Takei, A. Morisako, M. Matsumoto, J. Magn. Magn. Mater. **272–276**, 1703 (2004)
4. J. Sayama, K. Mizutani, T. Ariake, K. Ouchi, T. Osaka, J. Magn. Magn. Mater. **301**, 271 (2006)
5. Y. K. Takahashi, T. Ohkubo, K. Hono, J. Appl. Phys. **100**, 053913 (2006)
6. I. Kato, S. Takei, X. Liu, A. Morisako, IEEE Trans. Magn. **42**, 2366 (2006)
7. X. Liu, H. Zhao, Y. Kubota, J. -P. Wang, J. Phys. D **41**, 232002 (2008)
8. Y. Nukaga, M. Ohtake, F. Kirino, M. Futamoto, IEEE Trans. Magn. **44**, 2891 (2008)
9. M. Ohtake, Y. Nukaga, F. Kiriono, M. Futamoto, J. Cryst. Growth **311**, 2251 (2009)
10. M. Seifert, V. Neu, L. Schultz, Appl. Phys. Lett. **94**, 022501 (2009)
11. F. Hofer, IEEE Trans. Magn. **6**, 221 (1970)
12. K. Kamino, Y. Kimura, T. Suzuki, Y. Itayama, Trans. Jpn. Inst. Met. **14**, 135 (1973)
13. A. J. Perry, J. Less-Common Met. **51**, 153 (1977)
14. H. Okamoto, T. B. Massalski, *Binary Alloy Phase Diagrams* (ASM International, Ohio, 1990)
15. H. Ido, M. Nanjo, M. Yamada, J. Appl. Phys. **75**, 7140 (1994)
16. A. Pasturel, C. Colinet, C. H. Allibert, P. Hicter, A. G. Percheron, J. C. Achard, Phys. Status Solidi B **125**, 101 (1984)
17. R. P. van Ingen, R. H. J. Fastenau, E. J. Mittemeijer, J. Appl. Phys. **76**, 1871 (1994)
18. B. D. Cullity, *Elements of X-Ray Diffraction* (Addison-Wesley, Massachusetts, 1956)
19. T. Yanagawa, M. Ohtake, F. Kirino, M. Futamoto, EPJ Web Conf. **40**, 06007 (2013)
20. S. Derkaoui, C. H. Allibert, J. Less-Common Met. **154**, 309 (1989)